The modelling of Surface-Water photoreactions made easier: introducing the concept of 'equivalent monochromatic wavelengths'

The Modelling of Surface-Water Photoreactions Made Easier: Introducing the Concept of 'Equivalent Monochromatic Wavelengths'

Davide Vione

Dipartimento di Chimica, Università degli Studi di Torino, Via Pietro Giuria 5, 10125 Torino, Italy.

E-mail: *davide.vione@unito.it*

Abstract

The recent development of successful model approaches that predict the photochemical behaviour of surface waters has greatly aided in the understanding of how water environments work and will likely work in the future, from a photochemical point of view. However, the inherent multi-wavelength (polychromatic) nature of environmental photochemistry results into a mathematics that is quite complex, and discourages many scientists to carry out photochemical calculations. To greatly simplify model mathematics, this paper proposes a new approach that is based on a monochromatic approximation to the polychromatic problem, introducing the concept of what is here defined as equivalent monochromatic wavelengths (EMWs). The EMW is the single wavelength that reproduces the behaviour of the polychromatic system, using a monochromatic (Lambert-Beer based) equation. The EMW approach largely simplifies calculations, getting rid of integrals and allowing for much more straightforward and manageable equations to be obtained. In particular, this work shows that: *(i)* the EMW approach, although approximated, entails a negligible loss in accuracy compared to the exact polychromatic treatment of photochemical reactions; *(ii)* in

the case of direct photolysis, the quantum yield is to be replaced by an apparent photon efficiency that is not bound to be < 1 (quantum yields can actually be > 1 for chain reactions and few other cases, but this is not the point here); *(iii)* the monochromatic Lambert-Beer equations work in most cases once the EMW is identified, with the present exception of sunlight absorption by chromophoric dissolved organic matter (CDOM). The latter spans a very wide wavelength range (from 300 to at least 600 nm), which makes a single-wavelength treatment more difficult. However, a relatively small modification to the monochromatic Lambert-Beer equation allows for successfully using the EMW approach, in the case of CDOM as well. The near-perfect coincidence between polychromatic and EMW-based predictions of photodegradation kinetics is here shown for the pollutants atrazine, bentazone, carbamazepine, diclofenac, diuron and ibuprofen. Extension to additional compounds requires translation of the traditional, polychromatic language into the EMW one. Hopefully, this contribution will introduce a new paradigm in the mathematical description of photochemical reactions in environmental waters. It could also become a new and simple way to treat multi-wavelength systems in general photochemistry studies, thereby completely changing the way multi-wavelength problems are dealt with.

Keywords: polychromatic systems; Lambert-Beer monochromatic equations; photochemical modelling; natural attenuation of pollutants; numerical data fit.

1. Introduction

Natural attenuation processes that occur in surface waters play a very important role in the degradation of water pollutants. Although natural attenuation is not sufficient to prevent pollution, the impact of human activities on water environments would be much higher than is currently observed, were attenuation processes not operational (Schwarzenbach et al., 2006; Fenner et al., 2013). Photochemical reactions triggered directly or indirectly by sunlight are an important

component in natural attenuation, and they are particularly effective against dissolved, water-soluble biorecalcitrant compounds (Cermola et al., 2005; Young et al., 2013; Remucal et al., 2014; Vione et al., 2014; Trivella et al., 2015; Trawinski and Skibinski, 2017; Yassine et al., 2018). Such features are quite common among the so-called contaminants of emerging concerns (CECs), which end up in surface waters largely because of insufficient removal by wastewater treatment plants (WWTPs). Indeed, the use of the activated sludge step for pollutant degradation selects for compounds that are both biorecalcitrant (otherwise they would be biodegraded by bacteria) and water-soluble (otherwise they would attach to the biomass and end up in the separated sludge phase, not the aqueous one) (Castiglioni et al., 2006; Gao et al., 2012; Richardson and Ternes, 2014).

Photochemical reactions in surface waters can be divided into direct photolysis and indirect photochemistry. In the former, the pollutant absorbs sunlight and gets transformed as a consequence (Pace and Barreca, 2014). In indirect photoreactions, sunlight is absorbed by naturally-occurring photosensitisers (Chromophoric Dissolved Organic Matter or CDOM, nitrate and nitrite) to produce a range of reactive transient species: the hydroxyl radical; $^{\bullet}OH$; the carbonate radical, $CO_3^{\bullet-}$; singlet oxygen, $^1O_2$, as well as CDOM triplet states, $^3CDOM^*$ (Rosario-Ortiz and Canonica, 2016; McNeill and Canonica, 2016). The photogenerated reactive transients quickly reach steady-state concentrations due to the production-consumption budget; they react with pollutants to induce degradation, but this is generally a secondary consumption pathway. The radical $^{\bullet}OH$ is in fact mostly scavenged by Dissolved Organic Matter (DOM, not necessarily chromophoric) and by HCO_3^- and CO_3^{2-}, as well as by Br^- in saltwater; $CO_3^{\bullet-}$ is scavenged by DOM; $^3CDOM^*$ are mainly deactivated by ground-state O_2, in part to yield $^1O_2$; finally, $^1O_2$ is mainly quenched by collision with water molecules (Zepp et al., 1977a; Vione et al., 2014).

Photochemical reactions can be studied in the laboratory, although it is difficult to completely reproduce the natural environment under laboratory conditions (especially as far as water column depths are concerned). Recently, it has become possible to reliably model surface-water photoreactions, based on pollutant photoreactivity data (absorption spectra, direct photolysis

quantum yields, second-order reaction rate constants with $^{\bullet}OH$, $CO_3^{\bullet-}$, $^1O_2$ and $^3CDOM^*$) and on photochemically-relevant environmental factors (sunlight irradiance and spectrum, water chemistry and depth) (Zhou et al., 2018; Vione and Scozzaro, 2019). A major feature of environmental photochemistry is its multi-wavelength nature or polychromaticity. Indeed, a range of wavelengths occurs in all, solar radiation, photosensitiser absorption, and pollutant absorption. This means that light absorption and, as a consequence, photoreactivity calculations are multi-wavelength ones and are largely based on numerical integrals (Zepp et al., 1977b; Zepp et al., 1987; Bodrato and Vione, 2014). The main drawback of this state of things is that the procedures needed to compute photoreactions are not easy and require either *(i)* dedicated software, which is freely available but may have limitations or be difficult to customise (EPA, 2020; Vione, 2020), or *(ii)* the self-development of calculation spreadsheets, which requires advanced IT skills (Zhou et al., 2018). These difficulties are probably the main obstacle that has limited so far the diffusion of photochemistry modelling within the scientific community (Plane et al., 1987; Gerecke et al., 2001; Halladja et al., 2007; Bintou et al., 2015; Silva et al., 2015; Carena et al., 2017; Silva et al., 2019; Apell and McNeill, 2019).

It is also the author's opinion that photochemical modelling would be greatly simplified, were it possible to formulate a general equation that describes photoreaction kinetics without recurring to integrals. This paper shows that this goal can actually be reached: indeed, polychromatic environmental photoreactions are conducive to a monochromatic approximation, which allows for the formulation of the above-mentioned general equation. This approximation greatly simplifies computations, while entailing a negligible loss in accuracy. In other words, for every photoreaction (e.g., the production of $^1O_2$ by irradiated CDOM) it is possible to find a single monochromatic wavelength, which closely approximates the behaviour of the polychromatic system. Such wavelength is here defined as 'equivalent monochromatic wavelength' (λ_{eq}, or EMW). In this way, it is possible to use a monochromatic Lambert-Beer equation (or a slightly modified one, *vide infra*) to suitably approximate the photoreaction system. The EMW-based approach to photochemical

calculations that is presented here, could introduce a completely new paradigm for the description of environmental photoreactions. It could allow for highly simplified photochemical calculations, and eventually for a much higher number of scientists to have access to photochemical modelling.

2. Methods

The model calculations concerning the polychromatic systems were carried out by using the APEX software (Aqueous Photochemistry of Environmentally-occurring Xenobiotics). APEX predicts degradation kinetics and lifetimes in surface waters, based on parameters that describe pollutant photodegradation (absorption spectra, direct photolysis quantum yields, second-order reaction rate constants with $^{\bullet}OH$, $CO_3^{\bullet-}$, $^1O_2$ and $^3CDOM^*$), and on features that are connected with the photochemical reactivity of the aquatic environments (solar spectrum and irradiance, water chemistry and spectrum, depth of the water column) (Bodrato and Vione, 2014; Vione, 2020). To do so, APEX carries out multi-wavelength calculations that make wide use of numerical integrals (Braslavky, 2007), using polychromatic equations that will be presented later on, wherever relevant for the discussion. The use of APEX to do these calculations is simply much faster than carrying out numerical integrals one by one. Not all the quantities used in this work explicitly appear in the output files (e.g., APEX explicitly reports the steady-state concentrations of $^{\bullet}OH$, $CO_3^{\bullet-}$, $^1O_2$ and $^3CDOM^*$, but not their formation rates, *vide infra*), but one can obtain the desired data by applying suitable back calculations to the APEX output. Briefly, APEX produces .csv files that can be processed by, e.g., Microsoft Excel® to obtain the desired quantities.

The results of polychromatic calculations were plotted using the Fig.P software (Fig.P Software Corporation, Ontario, Canada). The same software was also used to fit the polychromatic data with monochromatic equations based on the Lambert-Beer law (Braslavky, 2007), which were slightly modified whenever necessary to improve the data fit (e.g., for CDOM absorption and related quantities). Basically, the form of the monochromatic equations (EMW approach) is similar to that

of the polychromatic ones, except that the EMW approach does not make use of integrals that, in fact, do not appear in the monochromatic Lambert-Beer law. The relevant polychromatic and EMW equations will be presented wherever required, in the next Results and Discussion section.

A suitable starting point to identify the EMW that best reproduces the behaviour of the polychromatic system, is to take water absorbance into account. The absorbance of surface waters is mostly accounted for by CDOM, especially in the 300-500 nm wavelength interval that is most significant for photochemical reactions (Bracchini et al., 2004; Galgani et al., 2011). On this basis, water absorbance can be expressed as follows: $A_w(\lambda) = 100 A_1(\lambda)\ DOC\ d$, where $A_w(\lambda)$ is unitless, $A_1(\lambda)$ has units of L mg_C^{-1} cm^{-1}, the DOC (dissolved organic carbon) is in mg_C L^{-1}, d (water depth) in m, and 100 is the conversion factor between [m] and [cm]. The parameter $A_1(\lambda_{eq})$ is the most useful fit parameter that allows for the identification of λ_{eq}, because the two quantities are univocally linked by the relationship $A_1(\lambda) = 0.45 e^{-0.015\,\lambda}$ that often holds for surface waters (λ is here expressed in nm) (Vione et al., 2010). Therefore, once $A_1(\lambda_{eq})$ is determined by data fit, it is quite easy to derive the value of λ_{eq}. The latter allows for fixing the other two important parameters that depend on the wavelength in the polychromatic approach: they are $p°(\lambda_{eq})$, the incident spectral photon flux density of sunlight and $\varepsilon_S(\lambda_{eq})$, the molar absorption coefficient of the substrate (pollutant) S (Bodrato and Vione, 2014; Vione, 2020).

By applying the data-fit procedure to the different processes (direct photolysis and reactions with $^{\bullet}OH$, $CO_3^{\bullet-}$, $^1O_2$ and $^3CDOM^*$) and by summing up the respective fit equations, one obtains an approximated EMW equation that expresses the pseudo-first order photodegradation rate constant of the relevant pollutant (k(S)). For ease of writing and suitability of software use (Excel® and MapleV®, *vide infra*), this single EMW equation was actually split into a set of individual equations that are more easily managed. The predictions of the EMW equation/set of equations were then compared with the results of APEX modelling. EMW calculations were carried out by means of .xls spreadsheets, which are here reported as part of the Supplementary Material

(hereinafter SM). To aid potential users, a dedicated spreadsheet is here provided for each studied pollutant.

Additionally, in order to show that the approximated EMW equation can be managed with plot-drawing software without too much sophistication, 3D plots of k(S) vs. DOC and d were drawn by using MapleV® (Waterloo software, Ontario, Canada). The Maple scripts that are needed to obtain the 3D plots are provided as SM, one for each studied pollutant.

The choice of pollutants for this work was guided by the availability of photoreactivity parameters and, at the same time, of comparison results between field data of photodegradation kinetics and APEX predictions. In other words pollutants were chosen, for which photoreactivity data in the field exist, which have already been reproduced well with APEX (this means that the chosen pollutants also need to have known values of photolysis quantum yield and second-order reaction rate constants with the photogenerated transients, otherwise predictions with APEX cannot be made). The available field data were thus used to validate the application of APEX to the relevant pollutants and, in turn, the approximated EMW predictions were validated by comparing them with the APEX results. The comparison between APEX predictions and field photoreactivity data is provided in **Table 1**, for the different pollutants under study.

Table 1. Comparison between model predictions of photodegradation lifetimes for the considered pollutants, and lifetimes observed in the field due to photochemical reactions, as obtained in previous studies (with one exception: the case of DIU was not a field study, rather natural lakewater has been irradiated under simulated sunlight). Model predictions were obtained by using the APEX software, with the water chemistry and depth parameters specified in the relevant field publications.

Compound	Acronym	Field lifetime (days, location)	Modelled lifetime (days) [a]
Atrazine	ATZ	20-21 & 67-100 (two sites in Patuxent river estuary, Maryland, USA) (McConnell et al., 2004)	17 ± 4 & 64 ± 18 (Marchetti et al., 2013)
Bentazon	BTZ	5-15 (Rhône delta, France) (Al Housari et al., 2011)	6-20 (Carena et al., 2020)
Carbamazepine	CBZ	100-230 (Greinfensee, Switzerland) (Tixier et al., 2003)	90-170 (De Laurentiis et al., 2012)
Diclofenac	DCL	8.3 (Greinfensee, Switzerland) (Tixier et al., 2003)	7-8 (Avetta et al., 2016)
Diuron	DIU	7-8.5 (water from Greinfensee, lab irradiated with simulated sunlight) (Gerecke et al., 2001)	7-12 (Fabbri et al., 2015)
Ibuprofen	IBU	60-110 (Greinfensee, Switzerland) (Tixier et al., 2003)	60 (Vione et al., 2011)

[a] The same modelled datum was obtained both by using APEX and by applying the monochromatic (EMW) approximation, because of negligible differences in numerical results between the two approaches.

3. Results and Discussion

3.1. Monochromatic approximations to the polychromatic problem

3.1.1. Indirect photochemistry

The formation rate of ^{3}CDOM* from irradiated CDOM can be computed by considering the polychromatic absorption of sunlight by CDOM itself (Braslavsky, 2007; Bodrato and Vione, 2014):

$$R_{^3CDOM*} = \frac{10}{d}\int_{\lambda} \Phi_{^3CDOM*}\, p°(\lambda)[1-10^{-100\,A_1(\lambda)\,DOC\,d}]d\lambda \qquad (1)$$

where: $R_{^3CDOM*}$ has units of [mol L^{-1} s^{-1}]; d [m] is the optical path length of sunlight in water (in a first approximation, it can be assimilated to the water depth) (Zepp et al., 1977; Bodrato and Vione, 2014); 10 = 1000/100 is the ratio of two conversion factors, *(i)* between [L] and [cm^3] (1000), and *(ii)* between [m] and [cm] (100); $\Phi_{^3CDOM*}$ [unitless, or mol Einstein^{-1}] is the photogeneration quantum yield of ^{3}CDOM* from CDOM; $p°(\lambda)$ [Einstein cm^{-2} s^{-1} nm^{-1}] is the spectral photon flux density of sunlight; $A_1(\lambda)$ [L mg$_C^{-1}$ cm^{-1}] is the specific absorbance of CDOM over an optical path length of 1 cm (often it is $A_1(\lambda) = 0.45\ e^{-0.015\lambda}$; Vione et al., 2010); finally, DOC [mg$_C$ L^{-1}] is the dissolved organic carbon.

Note that $\Phi_{^3CDOM*}$ is a wavelength-averaged value and its use is only an approximation, because *(i)* there is compelling experimental evidence that the quantum yield of ^{3}CDOM* generation by irradiated CDOM decreases as the wavelength increases (Marchisio et al., 2015), thus the ^{3}CDOM* quantum yield should read as $\Phi_{^3CDOM*}(\lambda)$, and *(ii)* different types of CDOM show different photoreactivity (Dong and Rosario-Ortiz, 2012; McNeill and Canonica, 2016, Wang et al., 2020).

However, presently available data concerning the wavelength trend of $\Phi_{^3CDOM*}(\lambda)$ are quite rough (they consist of just three figures, referred to the UVB, UVA and blue spectral ranges; Marchisio et al., 2015) and do not provide a considerable improvement over the use of just one average value. Work is currently in progress to obtain a more refined wavelength trend for $\Phi_{^3CDOM*}(\lambda)$, as well as for $\Phi_{^1O_2}(\lambda)$ and $\Phi_{^\bullet OH}(\lambda)$. Moreover, although different values of $\Phi_{^3CDOM*}$ have been reported upon irradiation of different CDOM specimens (McNeill and Canonica, 2016), the irradiation of natural water samples from quite different environments (lowland lakes of different trophicity, mountain lakes) has provided surprisingly small variability in $\Phi_{^3CDOM*}(\lambda)$ (Marchisio et al., 2015), perhaps suggesting that the same chromophores may be operational in different contexts. The most important differences have been observed upon irradiation of water samples taken soon after water de-icing, and thus relative to water that had undergone very little photo-processing prior to sampling (De Laurentiis et al., 2013). It might thus be suggested that a previous history of CDOM irradiation may play key role in defining photoreactivity, and that sunlight exposure might be a very effective equalizer as far as CDOM photoreactivity is concerned.

Starting from **Equation (1)**, it is interesting to see whether there is a single wavelength at which the photochemical behaviour of CDOM reproduces the polychromatic trend of, e.g., $R_{^3CDOM*}$ as a function of DOC and *d* (they are the most important water parameters as far as photochemistry is concerned) (Vione et al., 2014). The monochromatic (EMW) equation for $R_{^3CDOM*}$ should have a Lambert-Beer form, as follows (Braslavsky, 2007):

$$R_{^3CDOM*} = \frac{10}{d}\varphi_{app}(^3CDOM*)\ p°(\lambda_{eq})[1-10^{-100\,A_1(\lambda_{eq})\,DOC\,d}] \qquad (2)$$

where $p°(\lambda_{eq})$ [Einstein cm^{-2} s^{-1} nm^{-1}] is the spectral photon flux density of sunlight at the wavelength λ_{eq}, and $A_1(\lambda_{eq})$ [L mg_C^{-1} cm^{-1}] is the specific absorbance of CDOM at λ_{eq}. The

quantity $\varphi_{app}(^3CDOM^*)$ deserves additional explanation. It replaces the quantum yield $\Phi_{^3CDOM^*}$, but it is not exactly a quantum yield. It is rather the ratio between the reaction rate of a polychromatic process and the absorption of monochromatic radiation at λ_{eq}, in this case by CDOM. Because radiation absorption at a single wavelength is much lower than polychromatic absorption (which sums up absorption of radiation at all relevant wavelengths), it would not be surprising to find $\varphi_{app} > 1$ even if $\Phi < 1$. Hereinafter, φ_{app} will be named 'apparent photon efficiency'.

Figure 1a reports, as solid squares, the APEX (polychromatic) results for $R_{^3CDOM^*}$ as a function of both DOC (varied in a range of up to 25 $mg_C\ L^{-1}$) and *d* (up to 10 m), which conditions are relevant to most reasonably sunlit (i.e., not too deep or coloured) surface waters where photochemistry has good chances to be important (Vione et al., 2014). The polychromatic values were obtained by means of **Equation (1)**, considering a standard sunlight spectrum with UV irradiance (290-400 nm) of 22 W m^{-2}, as can be found in mid-July at mid-latitude, at 9 am or 3 pm solar time (it is the default spectrum used in APEX, see also **Figure S1** in SM) (Bodrato and Vione, 2014; Vione, 2020). The dashed curves represent the fit of the polychromatic data with **Equation (2)** (EMW approximation), with the constraint of matching λ_{eq} between $p°(\lambda_{eq})$ and $A_1(\lambda_{eq})$ (that is, the two quantities should correspond to the <u>same</u> wavelength that, when found, is defined as λ_{eq} or EMW). The same value of λ_{eq} (500 nm in the present case) was used for all the fit curves: this means that optimisation was done on the intermediate data set (that corresponding to d = 3 m), and the optimised results were then applied to all the other sets, with *d* as the only variable. The fit quality is here acceptable (photochemistry modelling is affected by higher uncertainties), but not impressive. The main issue is that the polychromatic and the monochromatic functions have different curvatures, because penetration of sunlight into the water column is not the same at all wavelengths. Therefore, shorter wavelengths play a more important role at low *d*, and longer wavelengths become prevalent at high *d*. The Lambert-Beer monochromatic approximation, with a

single value of the specific water absorbance ($A_1(\lambda_{eq})$), cannot reproduce well such a polychromatic behaviour. To improve the quality of the approximation, one should find a way to enable the monochromatic equation to assume different curvatures at different depths, which cannot be done in the sheer Lambert-Beer monochromatic form that affords only a single curvature.

A suitable solution to this problem is to modify **Equation (2)** by adding an exponent, which depends on *d* and provides the needed change in curvature as *d* changes. Note that this exponent has no physical meaning: it is only a way to make the monochromatic equation adjust its curvature as *d* varies. Nevertheless, it is a quite easy way to maintain the monochromatic form while, at the same time, emulating the features of the polychromatic equation. By playing a bit with data fit, it was found that a suitable fit function has the following form:

$$R_{3_{CDOM*}} = \frac{10}{d}[\varphi_{app}(^3CDOM*)]\ p°(\lambda_{eq})\left[1-10^{-100\,A_1(\lambda_{eq})\,DOC\,d}\right]^{(\alpha d^2+\beta d+\gamma)} \qquad (3)$$

With λ_{eq} = 560 nm, $\alpha = -3.0\times10^{-4}$ m^{-2}, $\beta = 2.2\times10^{-4}$ m^{-1}, $\gamma = 0.58$ and $\varphi_{app}(^3CDOM*) = 0.33$, one gets the very good data fit that is reported as the dashed curves in **Figure 1b**. **Equation (3)** is only phenomenological, derived by a modification of the Lambert-Beer function, but it predicts the polychromatic trend very well at all values of DOC and *d* (note that $p°(560\text{nm}) = 3.3\times10^{-10}$ Einstein cm^{-2} s^{-1} nm^{-1}, and $A_1(560\text{nm}) = 1.0\times10^{-4}$ L mg$_C^{-1}$ cm^{-1}). Moreover, one has $\varphi_{app}(^3CDOM*)$ » $\Phi_{^3CDOM*}$ because of the monochromatic approximation.

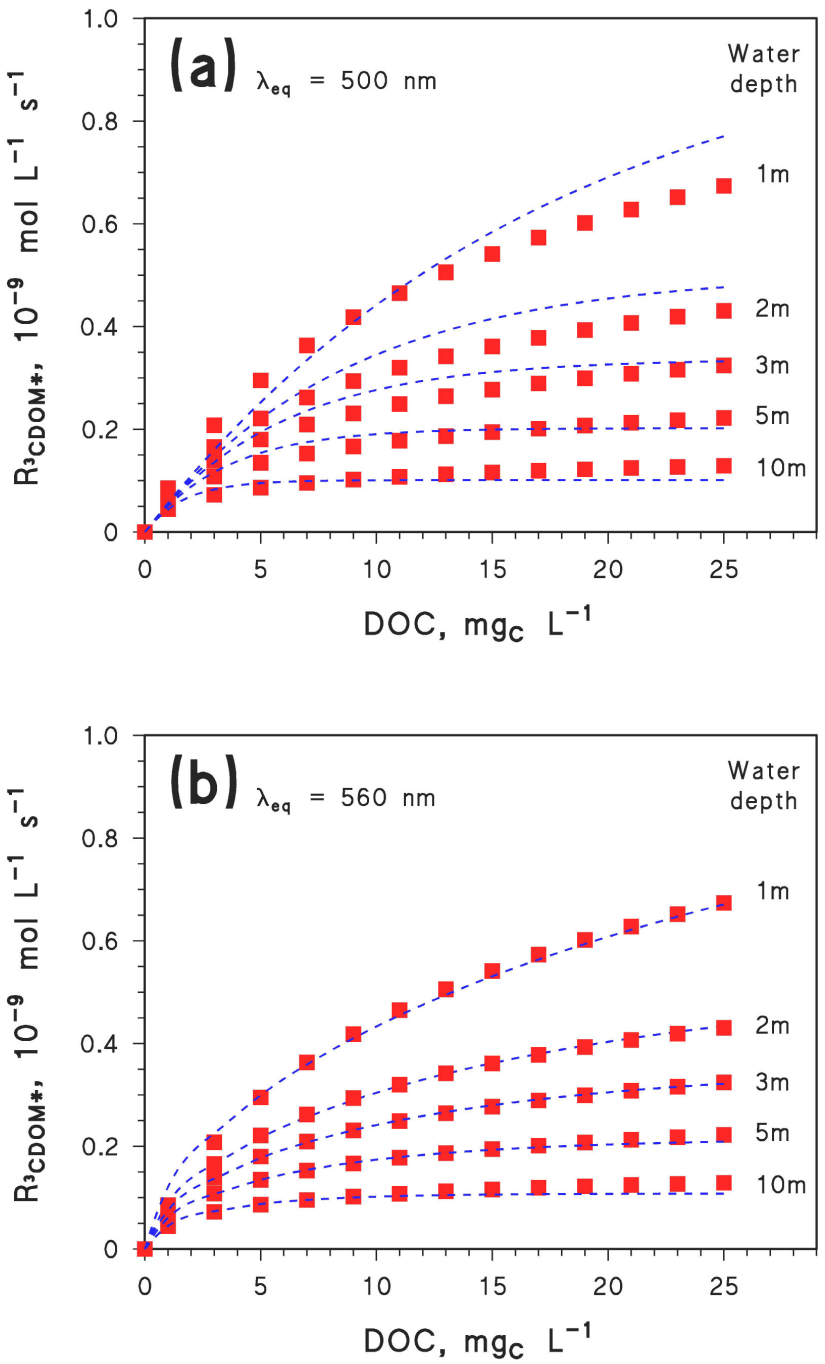

Figure 1. Solid squares: polychromatic data of $R_{^3CDOM*}$ vs. DOC and *d*, predicted by using the APEX software (***Equation 1***; note that the standard APEX output yields [^{3}CDOM*], which requires additional calculations to derive $R_{^3CDOM*}$ = [^{3}CDOM*] k_d, with $k_d = 5\times10^5$ s^{-1}) (Bodrato and Vione, 2014). The dashed curves represent the EMW predictions, obtained by using ***Equation (2)*** **(a)** and ***Equation (3)*** **(b)**. The used sunlight irradiance and spectrum corresponds to fair-weather 15 July at 45°N latitude, at 9 a.m. or 3 p.m. solar time (the APEX default) (Bodrato and Vione, 2014). Other water conditions: 10^{-4} mol L^{-1} NO_3^-, 10^{-6} mol L^{-1} NO_2^-, 10^{-3} mol L^{-1} HCO_3^-, and 10^{-5} mol L^{-1} CO_3^{2-}. The EMW values were λ_{eq} = 500 nm **(a)** and 560 nm **(b)**.

In the case of $^1O_2$, the polychromatic calculation of its formation rate reads as follows (see solid squares in **Figure 2a**) (Braslavsky, 2007; Bodrato and Vione, 2014):

$$R_{^1O_2} = \frac{10}{d}\int_{\lambda} \Phi_{^1O_2}\, p°(\lambda)[1-10^{-100 A_1(\lambda)\, DOC\, d}]\, d\lambda \tag{4}$$

Because $^1O_2$ is photogenerated by irradiated CDOM, like ^{3}CDOM*, the EMW approximation assumes the form already seen, with exponent added:

$$R_{^1O_2} = \frac{10}{d}[\varphi_{app}(^1O_2)]\; p°(\lambda_{eq})\left[1-10^{-100\, A_1(\lambda_{eq})\, DOC\, d}\right]^{(\alpha d^2+\beta d+\gamma)} \tag{5}$$

where λ_{eq}, $p°(\lambda_{eq})$, $A_1(\lambda_{eq})$, α, β and γ are the same as already seen for $R_{^3CDOM*}$ (which is reasonable, because CDOM is the light-absorbing species for both ^{3}CDOM* and $^1O_2$), while $\varphi_{app}(^1O_2)$ = 0.32. The predictions of **Equation (5)** with these parameters are shown as the dashed curves in **Figure 2a**, in quite good agreement with polychromatic **Equation (4)**.

The radical $^{\bullet}$OH can be generated by CDOM, NO_3^- and NO_2^-. The formation rate of $^{\bullet}$OH by CDOM reads as follows in, respectively, the polychromatic (Braslavsky, 2007; Bodrato and Vione, 2014) and EMW approaches:

$$R_{^{\bullet}OH}(CDOM) = \frac{10}{d}\int_{\lambda} \Phi_{^{\bullet}OH}(CDOM)\, p°(\lambda)[1-10^{-100 A_1(\lambda)\, DOC\, d}]\, d\lambda \tag{6}$$

$$R_{^{\bullet}OH}(CDOM) = \frac{10}{d}[\varphi_{app}(^{\bullet}OH, CDOM)]\; p°(\lambda_{eq})\left[1-10^{-100\, A_1(\lambda_{eq})\, DOC\, d}\right]^{(\alpha d^2+\beta d+\gamma)} \tag{7}$$

with the usual values of λ_{eq}, $p°(\lambda_{eq})$, $A_1(\lambda_{eq})$, α, β and γ, and with $\varphi_{app}(^{\bullet}OH, CDOM)$ = 7.7×10^{-3}.

The exponent $\alpha d^2 + \beta d + \gamma$ is the same as for ^{3}CDOM* and $^1O_2$, because CDOM is also in this case the photosensitiser that yields $^{\bullet}$OH. The agreement between the EMW and polychromatic results is again quite good (see **Figure 2b**).

Note that the same formal approach (formation quantum yield times CDOM absorption) was used here for the formation rates of ^{3}CDOM*, $^1O_2$ and $^\bullet$OH by irradiated CDOM. However, there is an important difference between the formation pathway of $^\bullet$OH and that of ^{3}CDOM*/$^1O_2$ (^{3}CDOM*/$^1O_2$ share the involvement of ^{3}CDOM*, although the wavelength trends are quite different: Marchisio et al., 2015; Partanen et al., 2020; this probably happens because some of the CDOM photosensitisers that produce $^1O_2$ might be unable to oxidise the ^{3}CDOM* probe molecules; McNeill and Canonica, 2016). Actually, $^\bullet$OH formation involves ^{3}CDOM* only to a partial extent. While water oxidation by ^{3}CDOM* is probably not an important $^\bullet$OH source, although some triplet states (but probably only a small minority of them) are actually able to oxidise H_2O and/or OH^- (Sur et al., 2011), about half of $^\bullet$OH photogeneration by CDOM involves H_2O_2 that might well be generated by ^{3}CDOM* reactions (see reactions 8-10, where S is an oxidisable organic molecule; Page et al., 2011). However, the other half of $^\bullet$OH photogeneration likely involves the photolysis of (poly)hydroxylated compounds that occur in irradiated CDOM (Sun et al., 2015), and here there is no clear evidence of ^{3}CDOM* involvement. Still, in all these cases the $^\bullet$OH photogeneration process is triggered by irradiated CDOM, which justifies the approach of "formation quantum yield times CDOM absorption" that was used here. It will be interesting to compare the detailed wavelength trends of $\Phi_{^3CDOM*}(\lambda)$ and $\Phi_{^\bullet OH}(\lambda)$ (work in progress), to see whether different pathways might result into different trends (currently available data suggest some similarities, but they are too few to enable proper comparison; Marchisio et al., 2015).

$$^3\text{CDOM*} + \text{S} \rightarrow \text{CDOM}^{\bullet-} + \text{S}^{\bullet+} \quad (8)$$

$$\text{CDOM}^{\bullet-} + \text{O}_2 \rightarrow \text{CDOM} + [\text{O}_2^{\bullet-} \leftrightarrows (\text{H}^+) \leftrightarrows \text{HO}_2^\bullet] \quad (9)$$

$$\text{HO}_2^\bullet + \text{O}_2^{\bullet-} + \text{H}^+ \rightarrow \text{H}_2\text{O}_2 + \text{O}_2 \quad (10)$$

In the case of nitrate and nitrite one should consider the fact that, unlike CDOM, these two species are not the main radiation absorbers in surface waters. Therefore, competition for sunlight between NO_3^-/NO_2^- and CDOM should be taken into account. The polychromatic and EMW treatments of the $^{\bullet}OH$ formation rates read, respectively, as follows (Braslavsky, 2007; Bodrato and Vione, 2014; Vione, 2020):

$$R_{^{\bullet}OH}(Sens) = \frac{10}{d}\int_{\lambda}\left\{[\Phi_{^{\bullet}OH}(Sens)]\,p^{\circ}(\lambda)\frac{\varepsilon_{Sens}(\lambda)[Sens]}{A_1(\lambda)\,DOC}[1-10^{-100\,A_1(\lambda)DOC\,d}]\right\}d\lambda \qquad (11)$$

$$R_{^{\bullet}OH}(Sens) = \frac{10}{d}[\varphi_{app}(^{\bullet}OH, Sens)]\,p^{\circ}(\lambda_{eq})\frac{\varepsilon_{Sens}(\lambda_{eq})[Sens]}{A_1(\lambda_{eq})\,DOC}\left[1-10^{-100\,A_1(\lambda_{eq})DOC\,d}\right] \qquad (12)$$

where *Sens* = NO_3^- or NO_2^-. In the case of NO_3^- it was: λ_{eq} = 315 nm; $\varphi_{app}(^{\bullet}OH, NO_3^-) = 0.86$; p°(315nm) = 1.8×10^{-11} Einstein cm^{-2} s^{-1} nm^{-1}; $\varepsilon_{NO_3^-}(315nm) = 5.2$ L mol^{-1} cm^{-1}, and A_1(315nm) = 4×10^{-3} L mg_C^{-1} cm^{-1}. In the case of NO_2^- it was: λ_{eq} = 360 nm; $\varphi_{app}(^{\bullet}OH, NO_2^-) = 1.4$; p°(360nm) = 7.8×10^{-11} Einstein cm^{-2} s^{-1} nm^{-1}; $\varepsilon_{NO_2^-}(360nm) = 22$ L mol^{-1} cm^{-1}, and A_1(360nm) = 2×10^{-3} L mg_C^{-1} cm^{-1}. The quite good agreement between the polychromatic and EMW calculations is reported in **Figure 2c** (NO_3^-) and **Figure 2d** (NO_2^-).

Interestingly, in the case of the photoproduction of $^{\bullet}OH$ by NO_3^- or NO_2^- as photosensitisers, there was no need to introduce an exponent in the EMW equation. This means that the Lambert-Beer equation at the right λ_{eq} reproduced well the polychromatic behaviour. The reason is that CDOM absorbs sunlight in a very wide wavelength interval (300-600 nm), where a pure Lambert-Beer law cannot predict absorption well at any single wavelength. In contrast, the wavelength range of sunlight absorption by NO_3^- (300-340 nm) and NO_2^- (300-420 nm) is more limited (Vione et al., 2007) and, as a consequence, more amenable to a EMW approach.

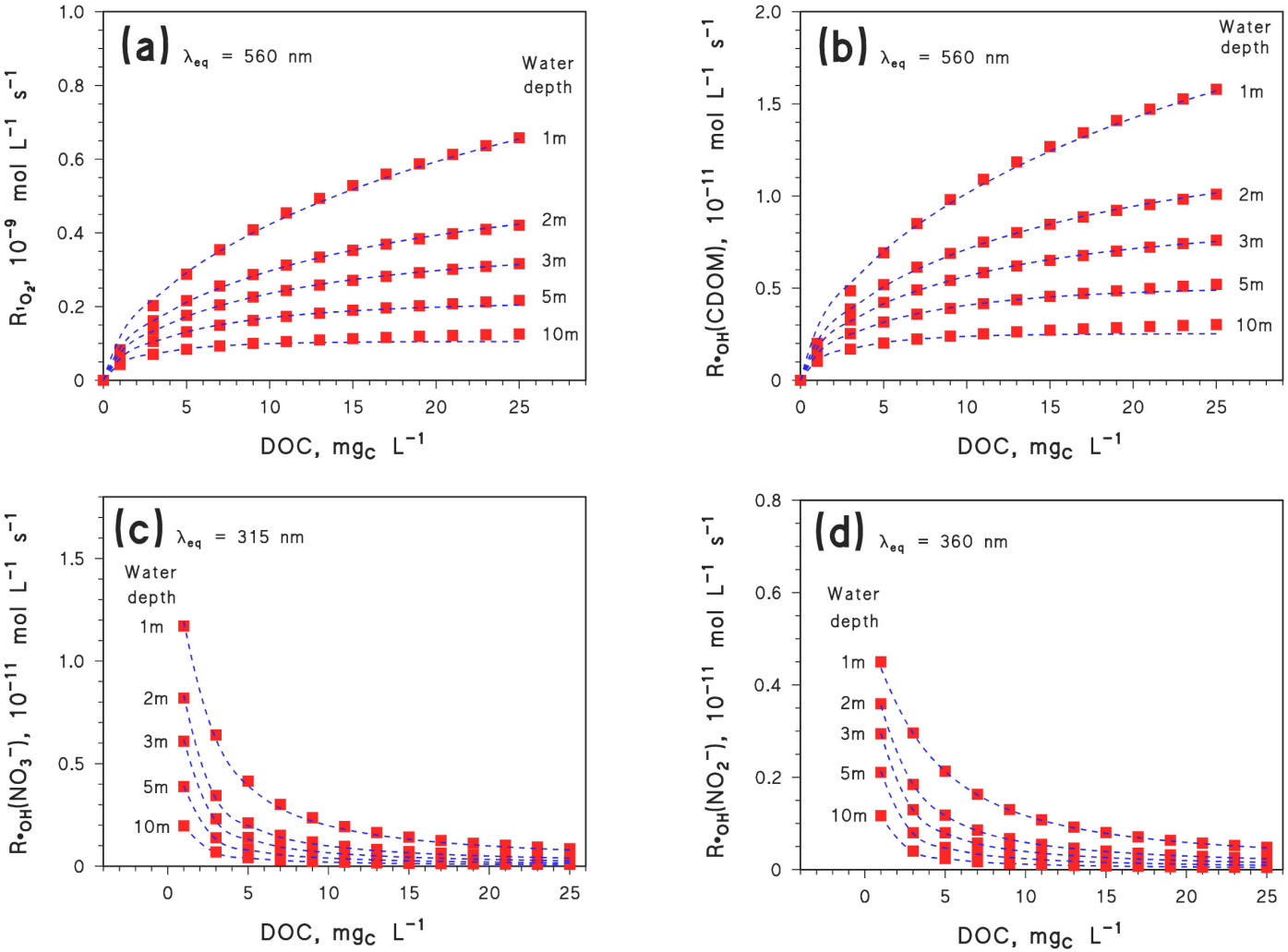

Figure 2. Solid squares: polychromatic APEX predictions of the formation rates of **(a)** $^1O_2$ (***Equation 4***); **(b)** $^\bullet OH$ by irradiated CDOM (***Equation 6***); **(c)** $^\bullet OH$ by irradiated NO_3^- (***Equation 11***, with *Sens* = NO_3^-); **(d)** $^\bullet OH$ by irradiated NO_2^- (***Equation 11***, with *Sens* = NO_2^-). Dashed curves: EMW predictions obtained by using **(a)** ***Equation (5)*****; (b)** ***Equation (7)*****; (c)** ***Equation (12)***, with *Sens* = NO_3^-; **(d)** ***Equation (12)***, with *Sens* = NO_2^-. Environmental conditions: sunlight irradiance and spectrum corresponding to fair-weather 15 July at 45°N latitude, at 9 a.m. or 3 p.m. solar time, 10^{-4} mol L^{-1} NO_3^-, 10^{-6} mol L^{-1} NO_2^-, 10^{-3} mol L^{-1} HCO_3^-, 10^{-5} mol L^{-1} CO_3^{2-}, and negligible bromide.

It is also interesting to observe that the photochemical production rates of ^{3}CDOM*, $^1O_2$ and $^\bullet$OH by irradiated CDOM increased with increasing DOC, while the production rates of $^\bullet$OH by NO_3^- and NO_2^- had the opposite trend. The reason is that the absorption of radiation by CDOM is higher at higher DOC, due to the higher amount of CDOM in solution. At the same time, elevated CDOM efficiently out-competes NO_3^- and NO_2^- for radiation absorption, which means that NO_3^- and NO_2^- absorb radiation to a lesser extent at higher DOC, and produce less $^\bullet$OH as a consequence (Vione et al., 2014; Vione and Scozzaro, 2019).

3.1.2. Direct photolysis

The different pollutants/substrates under study (S = ATZ, BTZ, CBZ, DCL, DIU and IBU) undergo direct photolysis as well. The direct photolysis rate constant ($k_{d.p.}$) of a substrate S upon absorption of radiation over a range of wavelengths should consider competition for sunlight between S and CDOM. Therefore, the photolysis rate constant $k_{d.p.}(S)$ can be expressed as follows (Braslavsky, 2007; Bodrato and Vione, 2014):

$$k_{d.p.}(S) = \frac{10}{d}\int_{\lambda}\left[p^{\circ}(\lambda)\, \Phi^{S}_{d.p.}\, \frac{\varepsilon_S(\lambda)\tau}{A_1(\lambda)\,DOC}\left(1-10^{-100\,A_1(\lambda)\,DOC\,d}\right)\right] d\lambda \qquad (13)$$

where $\Phi^{S}_{d.p.}$ [unitless or Einstein mol^{-1}] is the direct photolysis quantum yield of the pollutant S, $\varepsilon_S(\lambda)$ [L mol^{-1} cm^{-1}] its molar absorption coefficient (see **Figure S1** in SM), and $\tau = 3.6\times10^4$ s day^{-1} the conversion factor between the standard kinetic unit under constant irradiation (s^{-1}, 22 W m^{-2} constant UV irradiance) and the inverse of a sunny day equivalent to mid-latitude 15 July (i.e., day^{-1}), taking the respective sunlight irradiances and the day-night cycle into account (Bodrato and

Vione, 2014; Vione, 2020). All the other quantities have been defined previously. The EMW approximation takes the following form:

$$k_{d.p.}(S) = \frac{10}{d}\, p°(\lambda_{eq})\, \varphi_{app}(d.p.,S) \frac{\varepsilon_S(\lambda_{eq})\tau}{A_1(\lambda_{eq})DOC}(1-10^{-100\,A_1(\lambda_{eq})\,DOC\,d}) \qquad (14)$$

where φ_{app}(d.p.,S) is the apparent photon efficiency for the direct photolysis of S. The monochromatic approximation to the polychromatic trend is as good as usual (see **Figure S2** in SM), and there was no need to add an exponent to **Equation (14)** to obtain a decent data fit. The reason is that the wavelength range where the pollutants under study absorb sunlight is reasonably limited (up to one hundred nm, but usually much shorter, see **Figure S1** in SM). Therefore, a pure monochromatic trend can approximate the polychromatic one well, provided that λ_{eq} is correctly identified/chosen. In particular, it was found λ_{eq} = 340 nm for ATZ, 350 nm for BTZ, 333 nm for CBZ, 320 nm for DCL, 310 nm for DIU, and 350 nm for IBU. The values of the other parameters ($p°(\lambda_{eq})$, $A_1(\lambda_{eq})$, $\varepsilon_S(\lambda_{eq})$) are provided in **Table S1 (SM)**.

3.2. Modelling of pollutants photodegradation kinetics: polychromatic vs. monochromatic approaches

The pseudo-first order rate constant for the photodegradation of S in surface waters can be expressed as the sum of the contributions of all photochemical processes (Bodrato and Vione, 2014; Vione, 2020):

$$k(S)[day^{-1}] = k_{d.p.}(S) + \tau\{k_{S+^{\bullet}OH}[^{\bullet}OH] + k_{S+^{3}CDOM*}[^{3}CDOM*] + k_{S+^{1}O_2}[^{1}O_2] + k_{S+CO_3^{\bullet-}}[CO_3^{\bullet-}]\} \quad (15)$$

The term $\tau = 3.6\times10^4$ s day^{-1} is required in the case of indirect photochemistry, because the products k_{S+J} [J] yield values in [s^{-1}], while $k_{d.p.}$(S) has already been defined in [day^{-1}] units. The values of the second-order reaction rate constants of the studied pollutants with $^{\bullet}$OH, ^{3}CDOM*, $^{1}O_2$ and $CO_3^{\bullet-}$ are reported in **Table S1 (SM)**. The steady-state concentrations of $^{\bullet}$OH, ^{3}CDOM* and $^{1}O_2$ can be expressed as a function of the formation rates defined previously (**Equations 3,5,7,12**), as follows (Vione et al., 2014; Bodrato and Vione, 2014):

$$[^{\bullet}\mathrm{OH}] = \frac{R_{^{\bullet}OH}(CDOM) + R_{^{\bullet}OH}(NO_3^-) + R_{^{\bullet}OH}(NO_2^-)}{k_{Scav}} \quad (16)$$

$$[^{3}\mathrm{CDOM*}] = \frac{R_{^{3}CDOM*}}{k_d} \quad (17)$$

$$[^{1}\mathrm{O_2}] = \frac{R_{^{1}O_2}}{k_q} \quad (18)$$

where $k_{Scav} = k_{\bullet OH+DOM}\,DOC + k_{\bullet OH+HCO_3^-}[HCO_3^-] + k_{\bullet OH+CO_3^{2-}}[CO_3^{2-}] + k_{\bullet OH+NO_2^-}[NO_2^-]$ $+ k_{\bullet OH+Br^-}[Br^-]$ is the scavenging rate constant of $^{\bullet}$OH by the main solution components (see **Table S1 (SM)** for the values of the relevant second-order reaction rate constants), $k_d = 5\times10^5$ s^{-1} is the decay constant of ^{3}CDOM* in aerated solution (mostly accounted for by interaction with molecular O_2), and $k_q = 2.5\times10^5$ s^{-1} is the $^1O_2$ quenching constant upon collision with the water solvent (Zepp et al., 1977; Buxton et al., 1988; Canonica and Freiburghaus, 2001; Bodrato and Vione, 2014; McNeill and Canonica, 2016).

The case of $CO_3^{\bullet-}$ is a bit different because the carbonate radical is not produced directly by the photosensitisers, but rather indirectly upon interaction between $^{\bullet}$OH/^{3}CDOM* and inorganic carbon ($^{\bullet}$OH + HCO_3^-, $^{\bullet}$OH + CO_3^{2-}, ^{3}CDOM* + CO_3^{2-}) (Canonica et al., 2005). Therefore, the steady-state $[CO_3^{\bullet-}]$ can be expressed as follows (Bodrato and Vione, 2014; Vione, 2020):

$$[CO_3^{\bullet-}] = \frac{[^{\bullet}OH](k_{\bullet OH+HCO_3^-}[HCO_3^-] + k_{\bullet OH+CO_3^{2-}}[CO_3^{2-}]) + \eta_{CO_3^{\bullet-}}[CO_3^{2-}]P_{a,CDOM}}{k_{CO_3^{\bullet-}+DOM}\;DOC} \qquad (19)$$

Here it was used $k_{CO_3^{\bullet-}+DOM} = 10^2$ L mg$_C^{-1}$ s^{-1}, which roughly agrees with past literature findings (Canonica et al., 2005) and also with a recent study (Yan et al., 2019). In particular, Yan et al. (2019) report that $k_{CO_3^{\bullet-}+DOM}$ varies in the range of 15-240 L mg$_C^{-1}$ s^{-1} for different DOM specimens, and it decreases with increasing E2/E3 (the ratio of water absorbance values at 250 and 365 nm). This finding means that $k_{CO_3^{\bullet-}+DOM}$ is higher if (C)DOM is more aromatic. The value of $k_{CO_3^{\bullet-}+DOM}$ has a key impact on $[CO_3^{\bullet-}]$, as shown in **Figure S3** of the SM. Therefore, all other conditions being equal, waters with highly aromatic DOM might have low $[CO_3^{\bullet-}]$.

Considering that $R_{^3CDOM*} = \varphi_{app}(^3CDOM^*)\;P_{a,CDOM}$, from **Equation (3)** one gets the following:

$$P_{a,CDOM} = \frac{10}{d}\;p°(560nm)\left[1-10^{-100\,A_1(560nm)\,DOC\,d}\right]^{(\alpha d^2+\beta d+\gamma)} \qquad (20)$$

with the values of α, β and γ obtained before. Moreover, considering the ratio between polychromatic and monochromatic absorption, one gets $\eta_{CO_3^{\bullet-}}$ = 1.7. Therefore, one can use **Equation (20)** to obtain the value of $P_{a,CDOM}$ which, replaced in **Equation (19)**, gives [$CO_3^{\bullet-}$].

Considering all the different photochemical processes, it is possible to derive the steady-state concentrations of the photoreactive transients (**Equations 16-19**) and substitute them, together with the direct photolysis rate constant (**Equation 14**), into **Equation (15)**, to finally obtain the EMW assessment of the pseudo-first order photodegradation rate constants of the studied compounds.

The polychromatic modelling of lifetimes is carried out efficiently by the APEX software, thus one can compare the polychromatic ("exact") and monochromatic ("approximate") approaches to rate constants and lifetimes. The comparison is shown in **Figure 3**, where the solid squares represent the APEX results and the dashed curves are the EMW predictions, obtained by using **Equation (15)**. Again, one observes quite good agreement for all the DOC and depth conditions, which cover a wide range of environmental values for surface waters (Wetzel, 2001). This finding means that it is possible to reliably model phototransformation reactions by using a monochromatic approach based on EMWs, which allows for simpler equations to be obtained without numerical integrals, and thus considerably simplifies the mathematical treatment of photochemical modelling.

Note the trend with a minimum of *k*(ATZ) vs. DOC in **Figure 3a** (and, to a lesser extent, that of *k*(DIU) vs. DOC in **Figure 3e**): such a trend is due to the fact that increasing DOC inhibits direct photolysis as well as $^{\bullet}OH$ and $CO_3^{\bullet-}$ reactions, while enhancing the $^3CDOM^*$ and $^1O_2$ processes. One observes a similar trend whenever the $^3CDOM^*$ (and/or $^1O_2$) reaction becomes sufficiently fast at high DOC (Marchetti et al., 2013; Vione et al., 2014).

The excellent agreement between the polychromatic approach and the EMW-based one ensures that the data used to validate the APEX (polychromatic) model (see **Table 1**) can also be used for a validation of the EMW approximation. Therefore, also the EMW approach is able to predict quite well the field data of pollutant photodegradation.

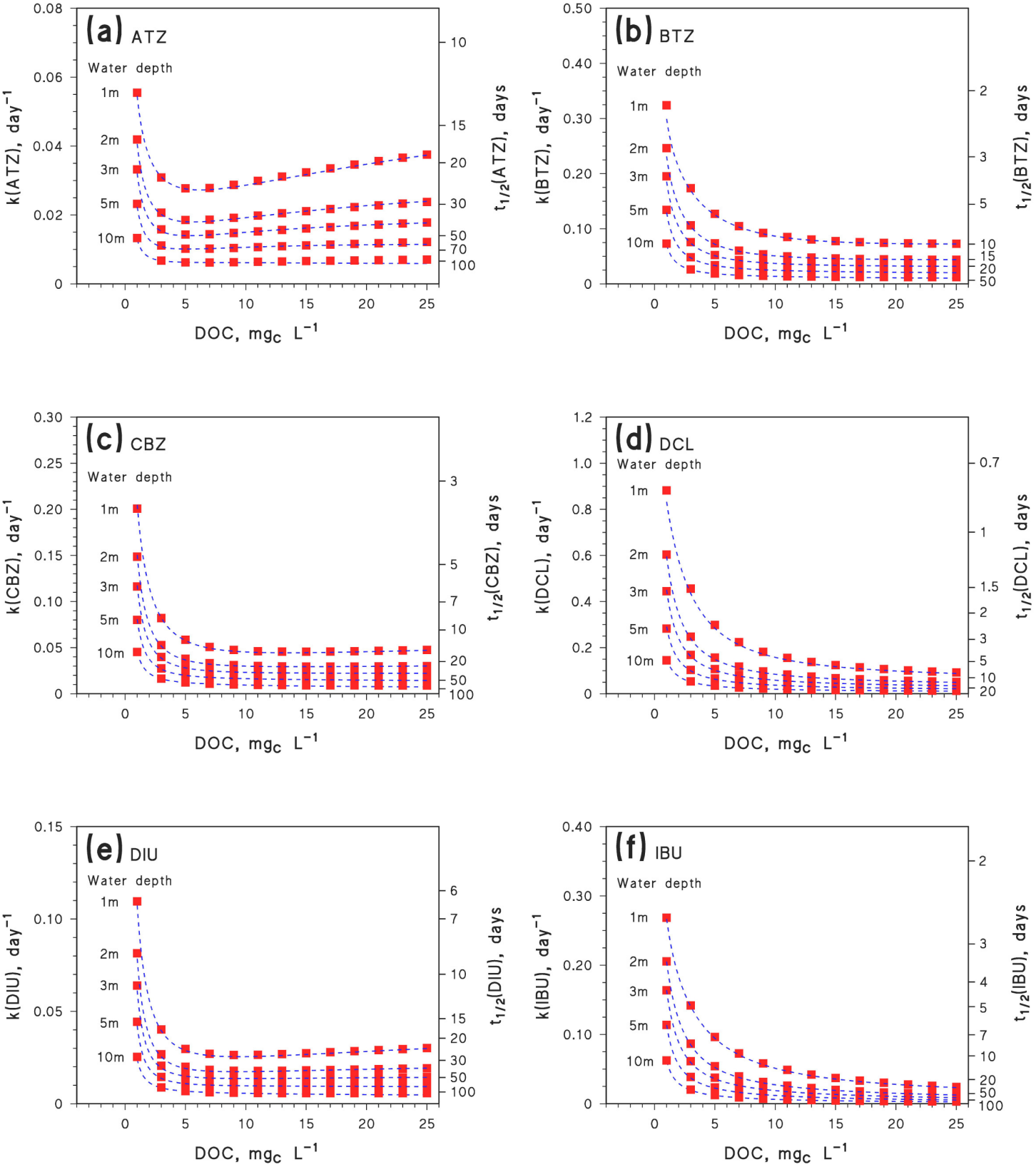

Figure 3. Solid squares: polychromatic data of the pseudo-first order degradation rate constant *k*, vs. DOC and *d*, predicted by using the APEX software for atrazine **(a)**, bentazone **(b)**, carbamazepine **(c)**, diclofenac **(d)**, diuron **(e)** and ibuprofen **(f)**. Dashed curves: EMW predictions for the relevant compounds (***Equations 14-20***). The spreadsheets used to carry out the EMW calculations are provided in the SM (file ***XLS.zip***). The used sunlight irradiance and spectrum corresponds to fair-weather 15 July at 45°N latitude, at 9 a.m. or 3 p.m. solar time (the APEX default). Other water conditions: 10^{-4} mol L^{-1} NO_3^-, 10^{-6} mol L^{-1} NO_2^-, 10^{-3} mol L^{-1} HCO_3^-, 10^{-5} mol L^{-1} CO_3^{2-}, and negligible bromide.

3.3. Implications for the modelling of freshwater photochemistry

It is the impression of the writer that the huge potential provided by photochemistry modelling, which also encompasses the relationship between surface-water photoreactions and climate change (Vione and Scozzaro, 2019), is presently exploited only in small part. One of the reasons may be that, thus far, modelling has made use of polychromatic calculations (which is fully justified, because the natural environment is indeed polychromatic) that are, however, quite difficult to implement. Therefore, one either has to use dedicated software (Bodrato and Vione, 2014; EPA, 2020; Vione, 2020), which often behaves as a 'black box' and may be difficult to customise, or has to develop own spreadsheets that have to include numerical integration procedures (Zhou et al., 2018). The latter require advanced programming skills that probably discourage many potential users.

This paper shows that it is possible to greatly simplify the mathematics and computational weight of the modelling process by replacing the polychromatic approach with a monochromatic one, based on EMWs, without significant loss in accuracy. Moreover, the ability of the EMW approach to carry out a reasonably correct prediction of the field lifetimes of two additional pollutants that do not undergo direct photolysis, such as the pharmaceutical metabolite and pesticide isomer clofibric acid and the artificial sweetener acesulfame K, is shown in **Table 2**.

Compared to polychromatic models, the EMW approach allows for a simpler set of mathematical equations to be obtained (the set of equations and their parameter values are summarised in the SM, **Table S1**), which can be included into a spreadsheet or into graphics software. Excel® spreadsheets to predict the first-order phototransformation rate constants and lifetimes of the studied pollutants are provided as SM. The SM also provides Maple V® scripts to draw 3D plots of the photodegradation rate constants vs. DOC and *d*. These 3D plots are shown in **Figure 4** for the different pollutants under study.

The present results constitute a 'proof of concept' that the EMW approach works well and is fully equivalent to the rigorous polychromatic treatment of photodegradation reactions, as far as

freshwater photochemistry is concerned. All calculations are here referred to mid-July, mid-latitude water conditions. The following implementations should be introduced in forthcoming work, to enable the adoption of EMW as the standard approach to surface-water photochemistry modelling:

(i) Extend the EMW approach to other contaminants, in particular as far as the direct photolysis is concerned. Indeed, each compound needs its own EMW treatment to find the values of λ_{eq} and φ_{app}(d.p.). For instance, the APEX database contains about 40 compounds in addition to those studied here (Vione, 2020), and it could constitute a good starting point for the work of 'translation' of the polychromatic language into the EMW one.

(ii) Extend the results to other latitudes and seasons. The present findings are limited to mid-July at mid latitude, because the used values of $p°(\lambda_{eq})$ and τ are referred to those conditions. $p°(\lambda_{eq})$ and τ are clearly functions of season and latitude (NCAR, 2015), and obtaining explicit forms for both would be the key to deriving a general, worldwide-valid equation for surface-water photochemistry.

As far as the former point is concerned, it is useful to get some insight into how to find the value of λ_{eq} that fits well the polychromatic data. Take such data, e.g., those of the direct photolysis rate constant vs. the DOC for different depths d (they are the data reported in **Figure S2** in SM; these data can be generated by APEX with the appropriate input values), and **Equation (14)** as the fit function. The curvature of the function is key to a good data fit, and it primarily depends on $A_1(\lambda_{eq})$. Therefore, one should first fit the polychromatic data of $k_{d.p.}$(S) vs. DOC with **Equation (14)** by fixing d and τ at their respective values, and by defining $A_1(\lambda_{eq})$, $p°(\lambda_{eq})$, φ_{app}(d.p.,S) and $\varepsilon_S(\lambda_{eq})$ as free-floating parameters. The obtained value of $A_1(\lambda_{eq})$ is the only important fit result, because it allows for λ_{eq} to be obtained from $A_1(\lambda) = 0.45\ e^{-0.015\lambda}$ ($\lambda = -66.7\ \ln(A_1(\lambda)) - 53.3$; note that $\ln(A_1(\lambda))$ varies from –5 to –8 in the range of 300-500 nm). That done, one can fix the values of $p°(\lambda_{eq})$ and $\varepsilon_S(\lambda_{eq})$. The next data fit can thus be carried out by taking only φ_{app}(d.p.,S) as free-floating variable. In this way, all the EMW parameters can be properly obtained. The last step is to

check that **Equation (14)** with the proper parameters predicts well the polychromatic results at all values of *d*.

Table 2. Comparison between the photochemical field lifetimes of clofibric acid and acesulfame K (Tixier et al., 2003; Zou et al., 2015), and the model predictions obtained with the EMW approach described in this work. The table also reports the photoreactivity parameters of the two compounds (second order reaction rate constants with $^{\bullet}OH$, $^{3}CDOM^{*}$ and $^{1}O_2$; Avetta et al., 2016; Minella et al., 2017), used for photochemical modelling.

	S = Clofibric acid	**S = Acesulfame K**
Type of compound	Degradation intermediate of clofibrate drugs and of the mecoprop herbicide	Artificial sweetener
$k_{S+^{\bullet}OH}$ **, L mol^{-1} s^{-1}**	7×10^{9}	$(5.9\pm2.0)\times10^{9}$
$k_{S+^{3}CDOM*}$ **, L mol^{-1} s^{-1}**	$(4.7\pm0.6)\times10^{8}$	Negligible
$k_{S+^{1}O_2}$ **, L mol^{-1} s^{-1}**	$(6.0\pm1.9)\times10^{5}$	$(2.8\pm1.1)\times10^{4}$
Photochemical field lifetime, days	>70	1200-1400
Field location	Greifensee, Switzerland	Norra Bergundasjön, Sweden
Photochemical, EMW-modelled field lifetime, days	77±26	1050±350

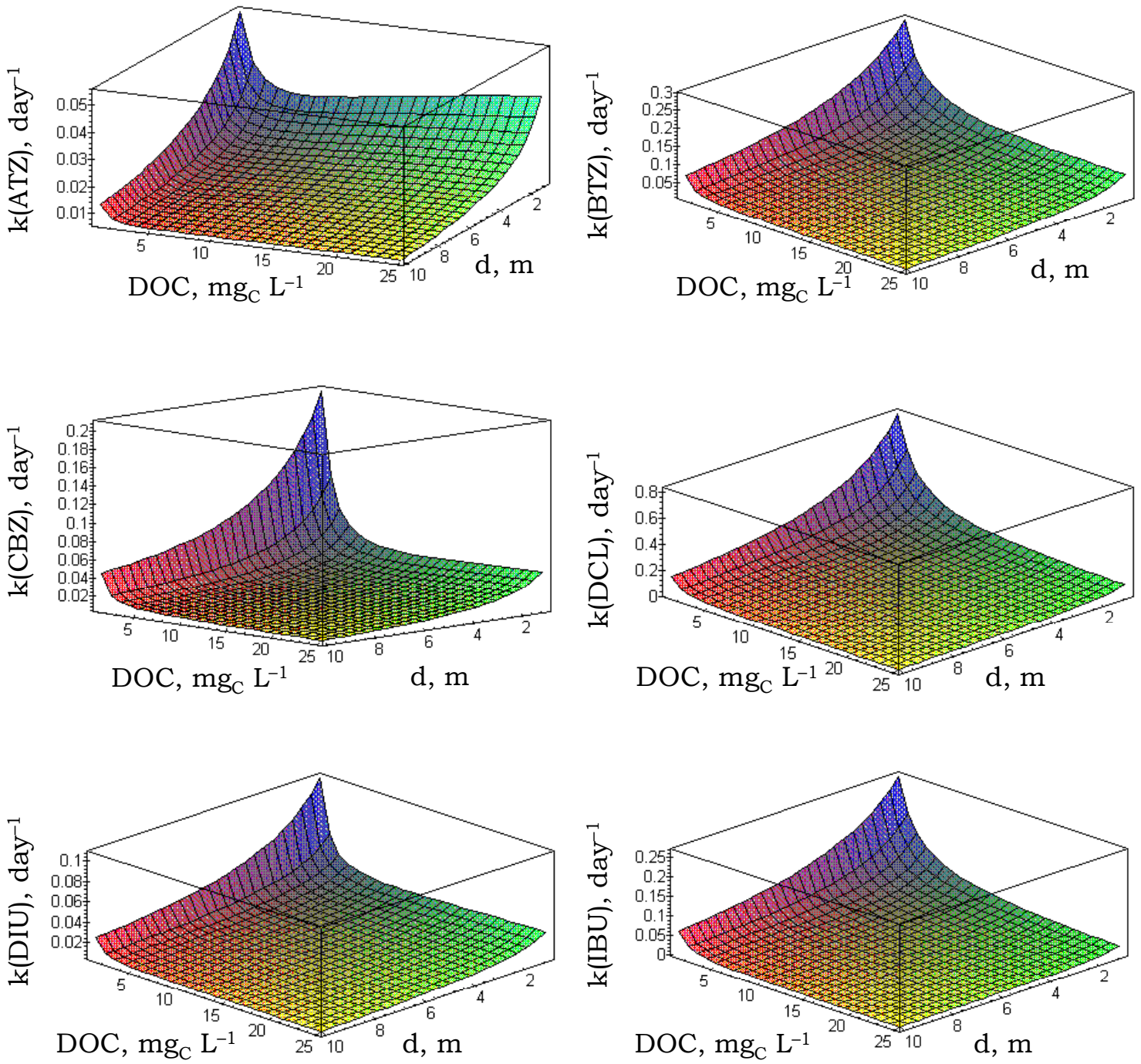

Figure 4. 3D graphs of the pseudo-first order degradation rate constant *k*, vs. DOC and *d*, predicted by using the MapleV® software for atrazine **(a)**, bentazone **(b)**, carbamazepine **(c)**, diclofenac **(d)**, diuron **(e)** and ibuprofen **(f)**. The Maple scripts used to obtain each of these plots are provided as SM (file ***Maple.zip***).

4. Conclusions

- An equivalent monochromatic wavelength (EMW) is here defined as the single wavelength that closely reproduces the behaviour of a polychromatic system. Once the EMW is found, it is possible to replace the polychromatic integrals with a much simpler, monochromatic Lambert-Beer equation, to derive radiation absorption and photoreaction rates.
- A pure EMW-based Lambert-Beer equation works less well in the case of CDOM absorption and related quantities. However, it is possible to solve the problem by introducing a slight modification to the Lambert-Beer equation, while maintaining its monochromatic nature.
- If the EMW language is adopted as standard in photochemistry calculations, it has the potential to greatly simplify computations of all polychromatic systems, including the photochemical processes taking place in the natural environment.

Supplementary Material Available. Additional Figures and Tables, cited in the main text (***.pdf file***); calculation spreadsheets for photodegradation kinetics (***XLS.zip***); MapleV scripts to draw 3D plots (***MapleV.zip***).

References

Al Housari, F., Höhener, P., Chiron, S., 2011. Factors responsible for rapid dissipation of acidic herbicides in the coastal lagoons of the Camargue (Rhône River Delta, France). Sci. Total Environ. 409, 582-587.

Apell, J. N., McNeill, K., 2019. Updated and validated solar irradiance reference spectra for estimating environmental photodegradation rates. Environ. Sci. Processes Impacts 21, 427-437.

Avetta, P., Fabbri, D., Minella, M., Brigante, M., Maurino, V., Minero, C., Pazzi, M., Vione, D., 2016. Assessing the phototransformation of diclofenac, clofibric acid and naproxen in surface waters: Model predictions and comparison with field data. Water Res. 105, 383-394.

Bintou, A. T., Bianco, A., Mailhot, G., Brigante, M., 2015. A new insight into ethoxyquin fate in surface waters: Stability, direct and indirect photochemical behaviour and the identification of main products. J. Photochem. Photobiol. A: Chem. 311, 118-126.

Bodrato, M., Vione, D., 2014. APEX (Aqueous Photochemistry of Environmentally occurring Xenobiotics): a free software tool to predict the kinetics of photochemical processes in surface waters. Environ. Sci.-Processes Impacts 16, 732-740.

Bracchini, L., Loiselle, S., Dattilo, A. M., Mazzuoli, S., Cozar, A., Rossi, C., 2004. The spatial distribution of optical properties in the ultraviolet and visible in an aquatic ecosystem. Photochem. Photobiol. 80, 139-149.

Braslavsky, S. E., 2007. Glossary of terms used in photochemistry. third edition. Pure Appl. Chem. 79, 293-465.

Buxton, G. V., Greenstock, C. L., Helman, W. P., Ross, A. B., 1988. Critical review of rate constants for reactions of hydrated electrons, hydrogen atoms and hydroxyl radicals ($^{\bullet}OH/^{\bullet}O^{-}$ in aqueous solution. J. Phys. Chem. Ref. Data 17, 513-886.

Canonica, S., Freiburghaus, M., 2001. Electron-rich phenols for probing the photochemical reactivity of freshwaters. Environ. Sci. Technol. 35, 690-695.

Canonica, S., Kohn, T., Mac, M., Real, F. J., Wirz, J., Von Gunten, U., 2005. Photosensitizer method to determine rate constants for the reaction of carbonate radical with organic compounds. Environ. Sci. Technol. 39, 9182-9188.

Carena, L., Fabbri, D., Passananti, M., Minella, M., Pazzi, M., Vione, D., 2020. The role of direct photolysis in the photodegradation of the herbicide bentazone in natural surface waters. Chemosphere 246, article n. 125705.

Carena., L., Minella, M., Barsotti, F., Brigante, M., Milan., M., Ferrero, A., Berto, S., Minero, C., Vione, D., 2017. Phototransformation of the herbicide propanil in paddy field water. Environ. Sci. Technol. 51, 2695-2704.

Castiglioni, S., Bagnati, R., Fanelli, R., Pomati, F., Calamari, D., Zuccato, E., 2006. Removal of pharmaceuticals in sewage treatment plants in Italy. Environ. Sci. Technol. 40, 357-363.

Cermola, M., DellaGreca, M., Iesce, M. R., Previtera, L., Rubino, M., Temussi, F., Brigante, M., 2005. Phototransformation of fibrate drugs in aqueous media. Environ. Chem. Lett. 3, 43-47.

De Laurentiis, E., Chiron, S., Kouras-Hadef, S., Richard, C., Minella, M., Maurino, V., Minero, C., Vione, D., 2012. Photochemical fate of carbamazepine in surface freshwaters: Laboratory measures and modeling. Environ. Sci. Technol. 46, 8164-8173.

De Laurentiis, E., Buoso, S., Maurino, V., Minero, C., Vione, D., 2013. Optical and photochemical characterization of chromophoric dissolved organic matter from lakes in Terra Nova Bay, Antarctica. Evidence of considerable photoreactivity in an extreme environment. Environ. Sci. Technol. 47, 14089-14098.

Dong, M. M., Rosario-Ortiz, F. L., 2012. Photochemical formation of hydroxyl radical from effluent organic matter. Environ. Sci. Technol. 46, 3788-3794.

EPA, 2020. *https://www.epa.gov/ceam/gcsolar*, last accessed in July 2020.

Fabbri, D., Minella, M., Maurino, V., Minero, C., Vione, D., 2015. Photochemical transformation of phenylurea herbicides in surface waters: A model assessment of persistence, and implications for the possible generation of hazardous intermediates. Chemosphere 119, 601-607.

Fenner, K., Canonica, S., Wackett, L. P., Elsner, M., 2013. Evaluating pesticide degradation in the environment: blind spots and emerging opportunities. Science 341, 752-758.

Galgani, L., Tognazzi, A., Rossi, C., Ricci, M., Angel Galvez, J., Dattilo, A. M., Cozar, A., Bracchini, L., Loiselle, S. A., 2011. Assessing the optical changes in dissolved organic matter in humic lakes by spectral slope distributions. J. Photochem. Photobiol. B: Biol. 102, 132-139.

Gao, P., Ding, Y., Li, H., Xagoraraki, I., 2012. Occurrence of pharmaceuticals in a municipal wastewater treatment plant: Mass balance and removal processes. Chemosphere 88, 17-24.

Gerecke, A. C., Canonica, S., Muller, S. R., Scharer, M., Schwarzenbach, R. P., 2001. Quantification of dissolved natural organic matter (DOM) mediated phototransformation of phenylurea herbicides in lakes. Environ. Sci. Technol. 35, 3915–3923.

Halladja, S., Ter Halle, A., Aguer, J.-P., Boulkamh, A., Richard, C., 2007. Inhibition of humic substances mediated photooxygenation of furfuryl alcohol by 2,4,6-trimethylphenol. Evidence for reactivity of the phenol with humic triplet excited states. Environ. Sci. Technol. 41, 6066-6073.

Marchetti, G., Minella, M., Maurino, V., Minero, C., Vione, D., 2013. Photochemical transformation of atrazine and formation of photointermediates under conditions relevant to sunlit surface waters: Laboratory measures and modelling. Water Res. 47, 6211-6222.

Marchisio, A., Minella, M., Maurino, V., Minero, C., Vione, D., 2015. Photogeneration of reactive transient species upon irradiation of natural water samples: Formation quantum yields in different spectral intervals, and implications for the photochemistry of surface waters. Water Res. 73, 145-156.

Mc Neill, K., Canonica, S., 2016. Triplet state dissolved organic matter in aquatic photochemistry: reaction mechanisms, substrate scope, and photophysical properties. Environ. Sci.-Processes Impacts 18, 1381-1399.

McConnell, L. L., Harman-Fetcho, J. A., Hagy, J. D., 2004. Measured concentrations of herbicides and model predictions of atrazine fate in the Patuxent river estuary. J. Environ. Qual. 33, 594-604.

Minella, M., Giannakis, S., Mazzavillani, A., Maurino, V., Minero, C., Vione, D., 2017. Phototransformation of Acesulfame K in surface waters: Comparison of two techniques for the measurement of the second-order rate constants of indirect photodegradation, and modelling of photoreaction kinetics. Chemosphere 186, 185-192.

NCAR (National Center for Atmospheric Research), 2015. Quick TUV calculator [WWW Document]. URL *http://cprm.acom.ucar.edu/Models/TUV/Interactive_TUV/* (last accessed in July 2020).

Pace, A., Barreca, S., 2014. Environmental organic photochemistry: Advances and perspectives. Curr. Org. Chem. 17, 3032-3041.

Page, S.E., Arnold, W.A., McNeill, K., 2011. Assessing the contribution of free hydroxyl radical in organic matter-sensitized photohydroxylation reactions. Environ. Sci. Technol. 45, 2818-2825.

Partanen, S. B., Erickson, P. R., Latch, D. E., Moor, K. J., McNeill. K., 2020. Dissolved organic matter singlet oxygen quantum yields: Evaluation using time-resolved singlet oxygen phosphorescence. Environ. Sci. Technol. 54, 3316-3324.

Plane, J. M. C., Zika, R. G., Zepp, R. G., Burns, L. A., 1987. Photochemical modeling applied to natural waters. In: Photochemistry of Environmental Aquatic Systems (ACS Symposium Series 327), Chapter 19, ACS, Washington DC, pp. 250-267.

Remucal, C. K., 2014. The role of indirect photochemical degradation in the environmental fate of pesticides: a review. Environ. Sci.-Process Impacts 16, 628-653.

Richardson, S. D., Ternes, T. A., 2014. Water analysis: emerging contaminants and current issues. Anal. Chem. 86, 2813-2848.

Rosario-Ortiz, F. L., Canonica, S., 2016. Probe compounds to assess the photochemical activity of dissolved organic matter. Environ. Sci. Technol. 50, 12532-12547.

Schwarzenbach, R. P., Escher, B. I., Fenner, K., Hofstetter, T. B., Johnson, C. A., von Gunten, U., Wehrli, B., 2006. The challenge of micropollutants in aquatic systems. Science 313, 1072-1077.

Silva, M. P., Acosta, A. M. L., Ishiki, H. M., Rossi, R. C., Mafra, R. C., Teixeira, A. C. S. C., 2019. Environmental photochemical fate and UVC degradation of sodium levothyroxine in aqueous medium. Environ. Sci. Pollut. Res. 26, 4393-4403.

Silva, M. P., Mostafa, S., McKay, G., Rosario-Ortiz, F. L., Teixeira, A. C. S. C., 2015. Photochemical fate of amicarbazone in aqueous media: Laboratory measurement and simulations. Environ. Engin. Sci. 32, 730-740.

Sun, L., Qian, J., Blough, N. V., Mopper, K., 2015. Insights into the photoproduction sites of hydroxyl radicals by dissolved organic matter in natural waters. Environ. Sci. Technol. Lett. 2, 352-356.

Sur, B., Rolle, M., Minero, C., Maurino, V., Vione, D., Brigante, M., Mailhot, G., 2011. Formation of hydroxyl radicals by irradiated 1-nitronaphthalene (1NN): Oxidation of hydroxyl ions and water by the 1NN triplet state. Photochem. Photobiol. Sci. 10, 1817-1824.

Tixier, C., Singer, H. P., Oellers, S., Mueller, S. R., 2003. Occurrence and fate of carbamazepine, clofibric acid, diclofenac, ibuprofen, ketoprofen, and naproxen in surface waters. Environ. Sci. Technol. 37, 1061-1068.

Trawinski, J., Skibinski, R., 2017. Studies on photodegradation process of psychotropic drugs: a review. Environ. Sci. Pollut. Res. 24, 1152-1199.

Trivella, A., Stawinoga, M., Dayan, F. E., Cantrell, C. L., Mazellier, P., Richard, C., 2015. Photolysis of natural β-triketonic herbicides in water. Water Res. 78, 28-36. DOI: 10.1016/j.watres.2015.03.026.

Vione, D., 2020. A critical view of the application of the APEX software (Aqueous Photochemistry of Environmentally-occurring Xenobiotics) to predict photoreaction kinetics in surface freshwaters. Molecules 25, article n. 9.

Vione, D., Das, R., Rubertelli, F., Maurino, V., Minero, C., Barbati, S., Chiron, S., 2010. Modelling the occurrence and reactivity of hydroxyl radicals in surface waters: implications for the fate of selected pesticides. Intern. J. Environ. Anal. Chem. 90, 260-275.

Vione, D., Maddigapu, P. R., De Laurentiis, E., Minella, M., Pazzi, M., Maurino, V., Minero, C., Kouras, S., Richard, C., 2011. Modelling the photochemical fate of ibuprofen in surface waters. Water Res. 45, 6725-6736.

Vione, D., Minella, M., Maurino, V., Minero, C., 2014. Indirect photochemistry in sunlit surface waters: photoinduced production of reactive transient species. Chem.-Eur. J. 20, 10590-10606.

Vione, D., Minero, C., Maurino, V., Pelizzetti, E., 2007. Seasonal and water column trends of the relative role of nitrate and nitrite as $^{\bullet}OH$ sources in surface waters. Ann. Chim. (Rome) 97, 699-711.

Vione, D., Scozzaro, A., 2019. Photochemistry of surface fresh waters in the framework of climate change. Environ. Sci. Technol. 53, 7945-7963.

Wang, H., Huaxi, Z., Ma, J., Nie, J., Yan, S., Song, W., 2020. Triplet photochemistry of dissolved black carbon and its effects on the photochemical formation of reactive oxygen species. Environ. Sci. Technol. 54, 4903-4911.

Wetzel, R. G., 2001. Limnology: Lake and River Ecosystems. Academic Press, Third Edition.

Yan, S., Liu, Y., Lian, L., Li, R., Ma, J., Zhou, H., Song, W., 2019. Photochemical formation of carbonate radical and its reaction with dissovled organic matters. Water Res. 161, 288-296.

Yassine, M., Fuster, L., Dévier, M.-H., Geneste, E., Pardon, P., Grélard, A., Dufourc, E., Al Iskandarani, M., Aït-Aïssa, S., Garric, J., Budzinski, H., Mazellier, P., Trivella, A. S., 2018. Photodegradation of novel oral anticoagulants under sunlight irradiation in aqueous matrices. Chemosphere 193, 329-336.

Young, R. B., Latch, D. E., Mawhinney, D. B., Nguyen, T.-H., Davis, J. C. C., Borch, T., 2013. Direct photodegradation of androstenedione and testosterone in natural sunlight: Inhibition by dissolved organic matter and reduction of endocrine disrupting potential. Environ. Sci. Technol. 47, 8416-8424.

Zepp. R. G., Wolfe, N. L., Baughman, G. L., Hollis, R. C., 1977a. Singlet oxygen in natural waters. Nature 267, 421-423.

Zepp, R. G., Cline, D. M., 1977b. Rates of direct photolysis in aquatic environment. Environ. Sci. Technol. 11, 359-366.

Zepp, R. G., Hoigné, J., Bader, H., 1987. Nitrate-induced photooxidation of trace organic chemicals in water. Environ. Sci. Technol. 21, 443-450.

Zhou, C. Z., Chen, J. W., Xie, H. J., Zhang, Y. N., Li, Y. J., Wang, Y., Xie, Q., Zhang, S. Y., 2018. Modeling photodegradation kinetics of organic micropollutants in water bodies: A case of the Yellow River estuary. J. Haz. Mat. 349, 60-67.

Zou, H., Radke, M., Kierkegaard, A., MacLeod, M., McLachlan, M. S., 2015. Using chemical benchmarking to determine the persistence of chemicals in a Swedish lake. Environ. Sci. Technol. 49, 1646-1653.